Neurocomputing 73 (2009) 179–190

Contents lists available at ScienceDirect

Neurocomputing

journal homepage: www.elsevier.com/locate/neucom

A graph matching approach for labeling brain sulci using location, orientation, and shape

Faguo Yang, Frithjof Kruggel

Signal and Image Processing Lab, Department of Biomedical Engineering, University of California, Irvine, USA

ARTICLE INFO

Available online 21 August 2009

Keywords:
Graph matching
Sulcus recognition
Human neocortex
Structural knowledge
Genetic algorithm

ABSTRACT

The human brain cortex is a highly convoluted sheet of gray matter composed of folds (gyri) and fissures (sulci). Sulci serve as important macroscopic landmarks to distinguish different functional areas of the brain. The exact segmentation and identification of sulci is critical for human brain mapping studies that aim at finding correspondences between structures and their function. In this paper, a sulcus identification algorithm is introduced using shape, orientation, location, and neighborhood information. Experimental results demonstrate that the method is efficient and accurate.

© 2009 Elsevier B.V. All rights reserved.

1. Introduction

The fissures (sulci) of the human brain (see Fig. 1) are important macroscopic landmarks that allow distinguishing different functional areas of the brain. An exact segmentation and identification of sulci has many applications in brain mapping studies: to build a brain atlas, to understand the individual variation of the local cortical geometry, to localize activation sites precisely in functional imaging, to describe morphological changes of brains affected by diseases, and to provide landmarks for nonlinear registration of brain image volumes.

However, segmenting and recognizing sulci is not a trivial task due to their considerable and well-known variability across subjects [24]. This variability can be broken down into three components: (1) Structure: differences in position, extent, and orientation of a specific sulcus are common. (2) Morphology: sulci may be continuous (found as one segment) or interrupted (found as multiple segments). In addition, some sulci are often connected. For example, the superior portion of the precentral sulcus is connected with the superior frontal sulcus in 100% on the left, in 92% on the right of the cases studied by Ono et al. [24]. A simple one-to-one correspondence between a segmented structure and an anatomically defined sulcus is (almost) never found. (3) Expression: some sulci may only be present in a subset of the population (refer to [24] for examples), and may confound the recognition of other sulci.

This problem has been the topic of many studies, and many algorithms were proposed to tackle this challenging identification problem. Let us distinguish these approaches by different ways of segmenting and representing the objects under study:

- Sulci segmented in 3D image space [9,18,20,28,29,41] or on a surface mesh [27,3,40,35,6].
- Sulci represented by points [20], curves [29,35,9,19], or regions [27,40,3].
- Sulci modeled by iconic (image-based) entities [9,35,20] or symbolic (feature-based) entities [28,3,29,33].

Initial approaches tried to segment and identify sulci in the (original) image space as sets of voxels. To recognize sulci, an iconic atlas isprovided, and nonlinear registration is used to match sulci with anatomical labels. While image-based approaches offer an advantage due to their simplicity, options for modeling the variability of structures are limited. Thus, pure iconic approaches (e.g., [9]) proved to be inefficient for dealing with the variability of the human neocortex.

More recent approaches use a (triangular) mesh that represents the brain surface to segment sulci. Although additional preprocessing steps are required, surface-based methods offer several advantages: (1) sulci are surface structures, and constraining the problem reduces the amount of data processing. (2) Surface features (e.g., curvature, distance) are more reliably computed, and multi-resolution schemes are much easier to implement that increase the robustness and computational efficiency. (3) Topological constraints on the surface may be imposed that are advantageous for sulcus segmentation and identification. (4) It is easier to generate a surface that closely resembles an anatomically relevant interface than to achieve such a segmentation in voxel space. Therefore, we use surface meshes that represent the interface of the brain's white and grey matter (WM/GM) that are reliably segmented [21,13].

Considerably high recognition rates for major sulci were achieved by a surface-based approach that uses a surface-based atlas and a nonlinear registration method that takes curvature and distance information on the cortical surface into account [6]. However, the problem of infrequently expressed sulci cannot easily be dealt with in this environment.

E-mail address: faguo.yang@STJUDE.org (F. Yang).

0925-2312/$ - see front matter © 2009 Elsevier B.V. All rights reserved.
doi:10.1016/j.neucom.2008.09.031

To overcome problems with example-based atlases, other authors try to abstract from the iconic level and recognize sulci at a higher abstraction level. Sulci were represented as locally deepest points ("sulcal roots") [26], regions around sulcal roots ("sulcal basins") [20], superficial curves on the convex hull of the brain [29,35], bottom lines deep in the fissures [9,19], medial walls in the sulci [28], or surface patches representing sulcal segments [40]. The question is still open how much and which information is necessary at this higher level to achieve a successful identification, as no current method has provided satisfying recognition rates.

A straightforward approach represents sulcal substructures as points and their variance in a point distribution model [20] but achieves recognition rates of only up to 80%. However, only substructures of the sulci ("sulcal basins") are recognized, and their concatenation to anatomically relevant entities is unsolved. Characterizing sulci (or their substructures) by additional parametric features (e.g., orientation and shape) [22] or parameters of Haar transforms from sulcal lines [38] enhances recognition rates.

We represent sulcal (sub)segments by a rich structural context here, including location, orientation, and shape (using geometric moment invariants). Because the relative positioning of sulci is highly invariant, using neighborhood relationships is very advantageous for identification. A straightforward option for representing this information is a graph [39], in which nodes contain structural features of a sulcus and edges correspond to their neighborhood relationships. So the task of identifying sulci is transformed here into a (incomplete) graph matching problem of a graph derived from a specific subject with a model obtained from training subjects. Graph matching allows recognizing a set of sulci jointly instead of separately (using probabilistic boosting trees [38]) or locally (using neuronal networks [28]) and, thus, is less prone to propagate identification errors.

Our main contributions are: (1) We characterize brain sulci by structural features and neighborhood information. (2) We introduce a strategy to cut surface segments that span different sulci. (3) We provide an approach for labeling sets of sulci, using a symbolic representation in a graph, in which similarity measures based on sulcal features between the subject cortical surface and those of training models are jointly optimized using a genetic algorithm. These methods are described in detail in the following section. We demonstrate the performance of our algorithm in several experiments, and finally discuss our current results in terms of our goal: to provide an automatic labeling of human brain sulci.

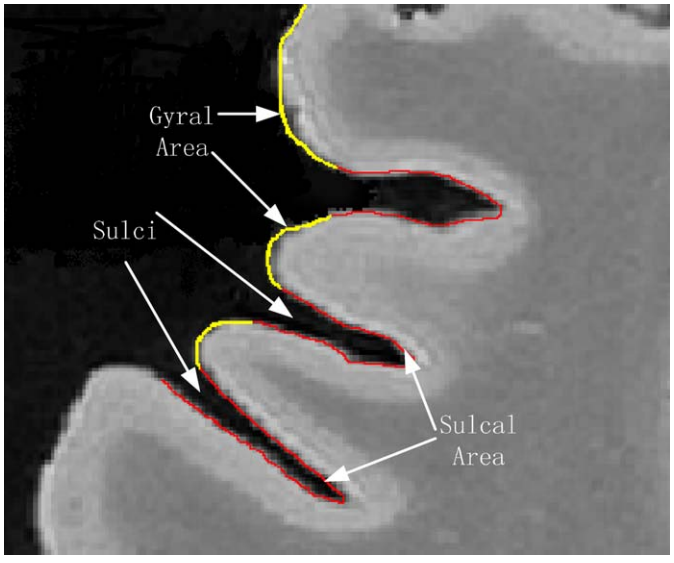

Fig. 1. A cross section of the cortical surface composed of folds (gyri) and fissures (sulci).

2. Method

2.1. Overview

The flowchart of the main steps is shown in Fig. 2. We start with a triangular surface that represents the WM/GM interface of the human brain [15]. Sulcal patches are obtained by segmenting the surface using information about local curvature and geodesic depth [40]. However, there is rarely a one-to-one correspondence between a patch and an anatomically defined sulcus. In some cases, segments must be merged to form a specific sulcus, in others, a segment must be split to separate connected sulci. First, we try to detect these latter cases and introduce a segment split. Then, we try to recognize a sets of segments as a specific sulcus in a subsequent labeling process.

A neuroanatomist manually labeled sulci in the training cases by sampling and cutting sulcal segments that were obtained automatically from surface segmentation. Shape, orientation, and location features were extracted that constitute the attribute descriptor of a sulcus. The relationship between neighboring sulci

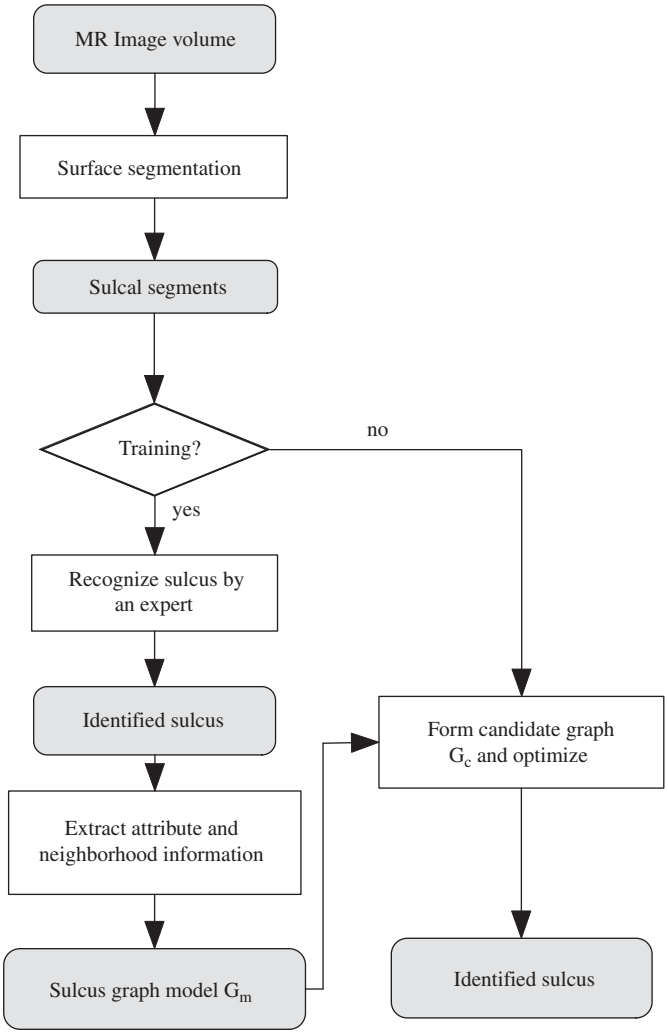

Fig. 2. Overview of the sulcus identification method.

was also extracted from the training set. All information is represented as a model graph G_m in which each node contains the attribute descriptors of a sulcus and edges indicate neighborhood relationships between sulci. To identify sulci for a new subject, we build a similar graph G_c from the subject's candidate sulcal segments and their neighborhood relationships. The similarity of G_m and G_c is maximized by selecting suitable candidates from the set of sulcal segments to form sulci in G_c. Finally, anatomical labels in G_m are addressed to successfully detected structures in G_c. Note that partial matches are possible, and some sulcal segments may remain unlabeled.

2.2. Spatial map

A specific sulcus is located in a relatively constant region on the cortical surface. We represent probabilistic information about sulcus extent in a spatial distribution model on a spherical map. At each location on this map, a vector contains the prior probabilities that this location belongs to a specific sulcus. We will take advantage of this knowledge to guide segment splits and to speed up optimization.

To generate this spherical map, we used the surface meshes from the training set, in which an expert labeled specific sulci. A mapping from each surface mesh onto a common sphere was computed. We employed a surface parametrization method to find the transformation function by minimizing a metric combining both angle and area distortion [15]. Hereby, each vertex on the set of manually labeled surface meshes received common coordinates on the unit sphere.

Consider N_t training subject hemispheres, vertex v on the common sphere, and φ a sulcus under study. The probability that vertex v belongs to φ is defined as

$$P_M(v \in \varphi) = \frac{1}{N_t}\sum_{i=1}^{N_t} X(T_i^{-1}(v), \varphi), \tag{1}$$

where T_i^{-1} corresponds to the transformation that maps the vertex v in the spherical space to its corresponding in hemisphere i, and $X(\overline{v}, \varphi)$ is a function defined as

$$X(\overline{v}, \varphi) = \begin{cases} 1 : \overline{v} \in \varphi, \\ 0 : \overline{v} \notin \varphi. \end{cases} \tag{2}$$

So each vertex on the common spherical map contains an array of probability values. Each value denotes a prior probability that this vertex belongs to a specific sulcus φ (see Fig. 3).

For a new subject under study, we determine the prior probabilities for all sulcal segments by mapping the WM/GM mesh onto the probabilistic atlas. The prior segment probability P that segment S belongs to a sulcus φ is given by

$$P(S \in \varphi) = \frac{1}{k_S}\sum_{i=1}^{k_S} P_M(T(\overline{v}_i) \in \varphi), \tag{3}$$

where k_S corresponds to the number of vertices that make up segment S, T is the transformation that maps vertex $\overline{v}$ onto the atlas in the spherical space. So $P(S \in \varphi_i)$ for $i = 1, \ldots, n_\varphi$ indicates in how much content segment S overlaps with the spatial distribution of sulcus φ_i.

Note that our mapping approach [15] does not depend on the selection of a pole and a split [1] that influence the final distortion of the map. Likewise, an initial inflation [37] is not required, that would result in an unspecified relation of the angles, distances, and areas of the brain mesh vs. the spherical map.

2.3. Surface segmentation and its graph representation

In this section, we introduce the generation of a WM/GM interface surface mesh, the segmentation of sulcal segments, segment cutting, and graph representation of the sulcal segments.

2.3.1. Surface generation

Extracting the WM/GM interface as a polygonal mesh from MR images of the human head is considered a complex but well developed methodology in medical image processing [11]. In principle, any published method may be used to compute a triangulated mesh that represents the WM/GM interface. However, it must be ensured that (1) the surface mesh has a topological genus of zero and (2) is free of self-intersections. It is self-evident that self-intersecting surfaces are anatomically invalid.

We briefly review our process for generating a WM/GM interface [13] here. A T_1-weighted volumetric MR image is registered with the stereotaxic coordinate system [16] and interpolated to an isotropical voxel size of 1 mm using a fourth-order B-spline method [36]. The dataset is segmented into three classes using a fuzzy c-means approach [25], and a raw segmentation of the white matter (WM) compartment is extracted, with the cerebellum and brainstem clipped away. The raw white matter segmentation is further refined to have a zero genus (i.e., no holes and handles) [31]. A triangulated surface mesh is generated from the refined WM segmentation using a topology-preserving variant of the "Marching Cubes" algorithm [5]. Finally, this initial mesh is optimized to match the WM/GM interface by treating it as a deformable model in the original image space [13].

2.3.2. Sulcus segmentation

Our method for generating sulcal segments is described in [40]. First, sulcal and gyral areas are classified using both geodesic depth and mean curvature information under a Bayesian framework. Then, a watershed region-growing method [23] is applied to form sulcal segments on the surface mesh.

2.3.3. Segment splitting

It is well known that some sulci are often connected, such as the superior portion of the precentral sulcus and the superior frontal sulcus [24]. Based on surface properties alone, it is impossible to separate such connected structures, but a proper cutting mechanism is required for a correct segmentation and recognition of sulci. It is not trivial to determine which segments must be split, because this already requires a successful identification. We use probabilistic information about the sulcal extent (see Section 2.2) here: if a segment overlaps with more than a single sulcus, it must be split.

Consider the simplified case of two connected sulci φ_1 and φ_2 (see Fig. 4) to illustrate our method. We aim at introducing splits in order to recognize them as separate entities. The segment under study is thinned to form a skeleton on the triangulated mesh (the broken lines in Fig. 4). In analogy to algorithms for hexahedral voxel meshes, a vertex is called simple if and only if its one-ring neighborhood contains both segment and non-segment vertices and each of the two sets forms one connected component (see Fig. 5). A vertex of the sulcal segment is an end vertex if and only if a single neighbor belongs to this segment. We also compute the geodesic depth of each vertex using a constrained distance transform (refer to [40] for details). Now, the steps to find the skeleton are spelled out as:

Step 1: Construct a list L of vertices v_i that belong to a sulcal segment and sort them in ascending order by their geodesic depth.

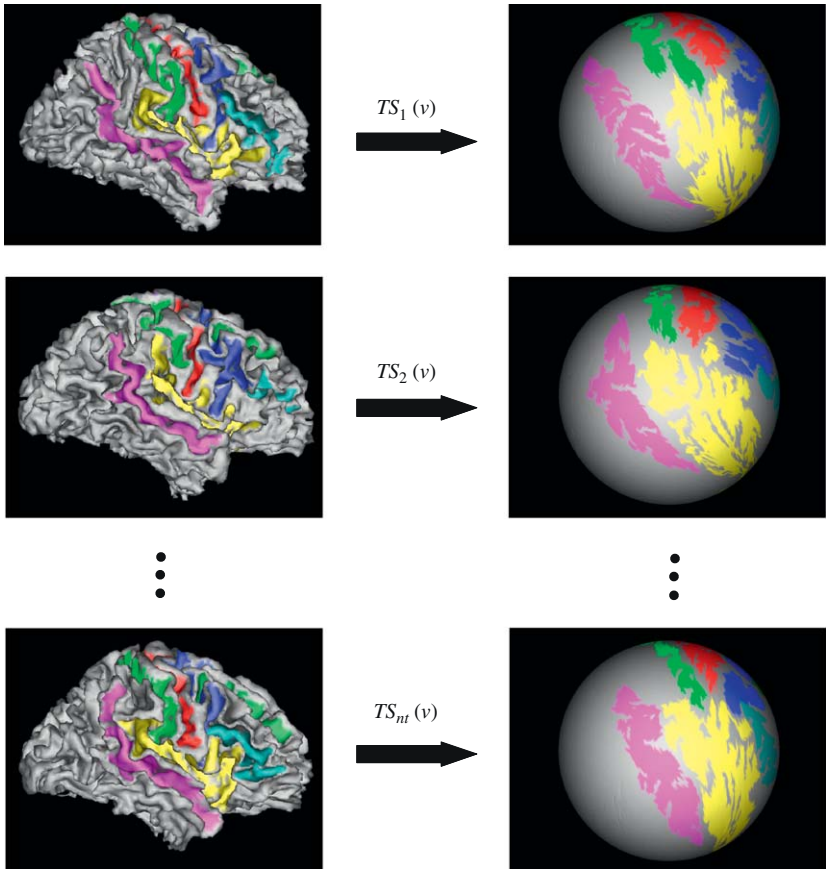

Fig. 3. A cortical surface (left) is mapped to a common unit sphere (right). A specific sulcus is mapped approximately to the same location on the sphere.

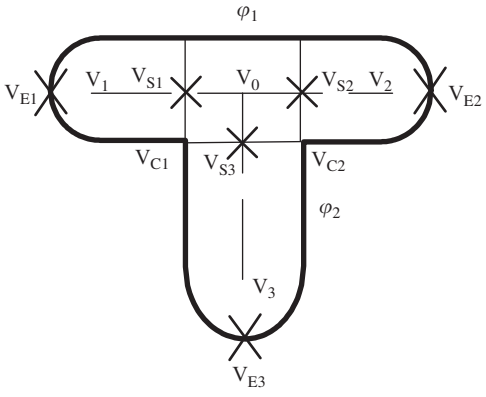

Fig. 4. Demonstration of the segment cutting method.

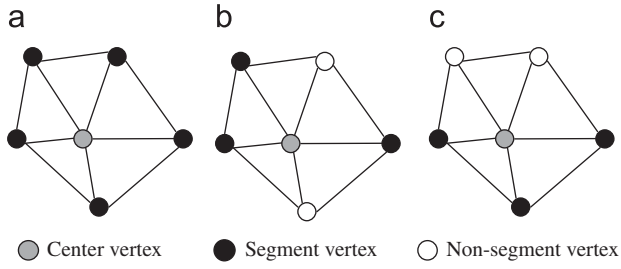

Fig. 5. Determination of simple vertex. In (a) the one-ring neighbors only contain object vertices, so the center vertex is not simple. In (b) the one-ring neighbors belonging to the object do not form a connected component, so the center vertex is still not simple. Only the center vertex in (c) is a simple vertex.

Step 2: Traverse through L and identify simple points. Remove these points from L.

Step 3: Repeat step 2 until no more simple points are found.

Step 4: Prune the skeleton based on length and connectedness with its neighbors [30].

Step 5: Form a spanning tree [2] of the remaining vertices in L.

Step 6: Find the pair of leaf nodes v_1 and v_2 of the spanning tree that has the maximum shortest path. Nodes between leaves v_1 and v_2 form the main branch of the skeleton.

Steps 7: Find the longest sub-branch that sprouts from the main branch, which together with the main branch form the skeleton (the broken line in Fig. 4).

Next, we track the boundary of the segment (the thick black outline in Fig. 4). The cross point v_0 of the skeleton is unique, because it has more than two neighbors, likewise, the three end points $v_{1,2,3}$ have a single neighbor only. Searching on the boundary for the closest point, v_{E1}, v_{E2}, and v_{E3} are identified. Then, we move v_0 along the skeletal segments $\overrightarrow{v_0v_1}$, $\overrightarrow{v_0v_2}$, and $\overrightarrow{v_0v_3}$ by a half of the sulcus width to obtain points v_{S1}, v_{S2}, and v_{S3}. Now, point sets $\{v_{Si}, v_{Ei}\}$ $(i = 1, 2, 3)$ are used to determine three paths that split the segment into several sub-segments. The exact number of the sub-segments depends on the relative positions of the splitting points. Consider $\{v_{S3}, v_{E3}\}$ as an example. We search for the point on the boundary that has the shortest distance to V_{S3}, denoted as v_{C1}. The other point v_{C2} of the splitting path $v_{C1}v_{C2}$ must be located on the opposite boundary segment $v_{E3}v_{E2}$ and have the shortest distance to v_{S3} (illustrated by a thin black line in Fig. 4). Note that the distance is measured on the vertex graph of the WM/GM surface mesh [2]. A connected segment is usually split into several sub-segments that do not necessarily correspond to anatomical entities. A split is considered as successful if each

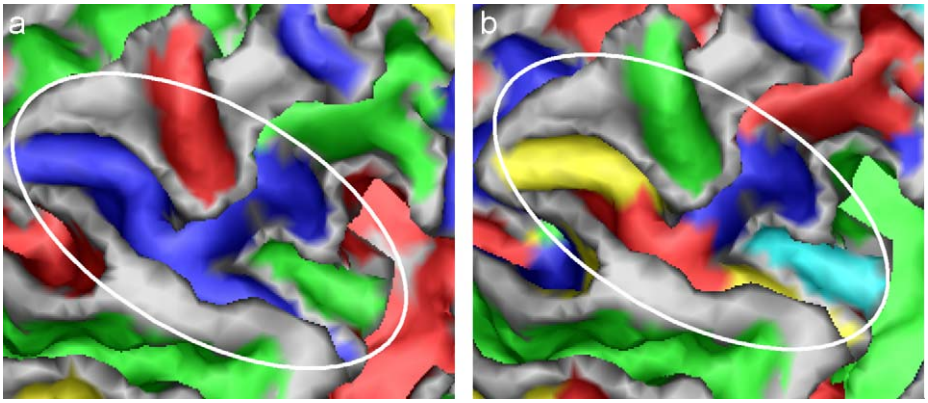

Fig. 6. Example results of the segment cutting procedure. The blue segment in the white ellipse in (a) is the original segment and the corresponding split segment is shown in (b). (For interpretation of the references to color in this figure legend, the reader is referred to the web version of this article.)

sub-segment belongs to a single sulcus only. In the later recognition process, we will merge any sub-segments that belong to the same sulcus. An example result of the splitting procedure is shown inFig. 6.

Our method cuts segment at branches. While it is possible that a long segment without ramifications spans over several sulci, we did not encounter such a (anatomically unlikely) case yet. The formation of long segments can be avoided by adjusting the watershed threshold in the sulcal segmentation step [40], i.e., by increasing the oversegmentation rate.

If sulci are represented as 3D curves, as in previous approaches [21,10], a connection is readily detected as a junction point. Because we deal with surface segments, the connection between two sulci corresponds to a 3D curve.

2.3.4. Graph representation of sulcal segments

Now that we found a set of sulcal segments on the brain surface, we construct a symbolic representation of this set as a graph, in which each node corresponds to a sulcal segment and edges indicate their neighborhood relationships.

Consider sulci mapped onto a sphere (see Fig. 3): sulcal segments may be regarded as "islands" in an "ocean" composed of gyral vertices. To find neighbors of a sulcal segment, we dilate segments on the mesh until no gyral vertices are left. The neighborhood relationship between two segments S_1, S_2 is quantified by the weight w that is determined from the number of dilation steps n_d (until they touch) and their average ridge height h_a:

$$w(S_1, S_2) = \exp(-(\alpha_1 n_d + \alpha_2 h_a)). \tag{4}$$

The average ridge height h_a can be calculated as

$$h_a = \frac{1}{N_p} \sum_{i=1}^{N_p} (r_{12}^i + r_{21}^i), \tag{5}$$

where N_p is the number of pairs of neighboring vertices between the two sulcal segments. The definition of r_{12}, r_{21} of neighboring vertices belonging to different sulcal segments is illustrated in Fig. 7.

Larger values of h_a and n_d yield a smaller weight $w(S_1, S_2)$. A larger weight results in a higher probability that segments S_1, S_2 are merged to form a sulcus.

2.4. Sulcus model graph

The model graph G_m that represents prior knowledge about structural features and neighborhood information of sulci is constructed from the set of N_t expert-labeled datasets.

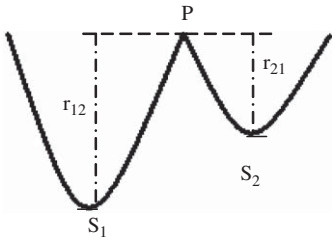

Fig. 7. The ridge height between neighboring vertices of sulcal segments S_1 and S_2 is defined as the geodesic depth measured from the convex hull of the mesh.

Let $\varphi_1, \ldots, \varphi_{n_\varphi}$ denote the n_φ sulci we want to recognize, which form the nodes of the graph model G_m. For each sulcus φ_i in each dataset of the training sample, we use location, orientation, and shape features collected in a feature vector $\vec{f}$ of dimension n_f. Because brain volumes are aligned with the stereotaxic coordinate system, orientation, and position information can be used for sulcus identification. To take account for brain size, positions are normalized by scaling the brain to fit into a bounding box of extent 1, centered at the origin of the coordinate system. We assume that components of the feature vector are independently Gaussian distributed, so we can represent node attributes for each sulcus φ_i in G_m by their means $\mu_1, \ldots, \mu_{n_f}$ and standard deviations $\sigma_1, \ldots, \sigma_{n_f}$. The edges of G_m indicates the neighboring relationships of the sulci.

2.4.1. Location information

Each sulcus usually is located in a relatively constant region of the cortical surface, so location is critical for the identification task. We use the centroid c_x, c_y, c_z of each segment to describe its location.

2.4.2. Shape information

Shape features are useful to distinguish sulci, as first demonstrated by Mangin et al. [22] and Sun et al. [34]. We use geometric moment invariants as descriptors of the sulcus shape. From the regular moments of order 0 to 2, 13 rotation-invariant moments are derived [17]. Suppose the origin of the coordinate system was shifted to the centroid of segment S composed of vertices v_S. A regular moment of order p, q, r for function $\rho(x, y, z)$ is defined as

$$M_{pqr} = \sum_{v \in \xi_S} x_v^p \, y_v^q \, z_v^r \, \rho(x_v, y_v, z_v). \tag{6}$$

Because we are interested in shape only, we simplify by setting $\rho(x, y, z) = 1$. The computation of the rotation-invariant descriptors from these moments is quite involved. We list only the first

four of them, and refer to [17] for complete information:

$$I_1 = M_{000}, I_2 = M_{200} + M_{020} + M_{002},$$
$$I_3 = M_{200}M_{020} + M_{200}M_{002} + M_{020}M_{002} - M_{101}^2 - M_{110}^2 - M_{011}^2,$$
$$I_4 = M_{200}M_{020}M_{002} - M_{002}M_{110}^2 + 2M_{110}M_{101}M_{011} - M_{020}M_{101}^2 - M_{200}M_{011}^2.$$

Note that M_{000} corresponds to the vertex count of segment S.

2.4.3. Sulcus orientation

We use the principal axes derived from the second-order moments to characterize the sulcus orientation. They are computed as the eigenvectors of the inertia tensor T:

$$T = \begin{bmatrix} M_{020}+M_{002} & -M_{110} & -M_{101} \\ -M_{110} & M_{200}+M_{002} & -M_{011} \\ -M_{101} & -M_{011} & M_{200}+M_{020} \end{bmatrix}.$$

There are up to three principal axes, because a real symmetric 3D matrix has up to three orthogonal eigenvectors. Denote $\vec{u}_{1,2,3}$ as the unit eigenvectors with corresponding eigenvalues $\lambda_1 < \lambda_2 < \lambda_3$. We select the most stable principal axis $\vec{u}_1$ to characterize the orientation. Because vectors $\vec{u}$ and $-\vec{u}$ are equivalent for sulcus identification, we choose the direction in one training subject as reference. Components of this vector are collected as the direction feature d_x, d_y, d_z.

2.4.4. Neighborhood information

To determine neighborhood information, sulcal segments obtained from the surface segmentation steps are dilated in each dataset of the training samples as described above. If two sulci φ_1 and φ_2 (made up of one or more sulcal segments) touch, they are considered as neighbors, and an edge is formed between their nodes with a weight $e_{12} = 1$. For the model graph G_m, weights between neighbors are averaged across the training samples:

$$\overline{e_{12}} = \frac{1}{N_t}\sum_{i=1}^{N_t} e_{12}(i). \tag{7}$$

2.5. Labeling sulci

In Section 2.3.4 we described the generation of a segment graph G_s derived from the WM/GM mesh of an individual subject. Note that G_s is fundamentally different from the model graph G_m, because nodes in G_s are sulcal segments, and nodes in G_m expert-recognized and labeled sulci. To perform a labeling process in G_s, we need to assemble sulcus candidates from segments in G_s, and compile them in a candidate graph G_c that is structurally equivalent to G_m and can be compared using a similarity function. So, the process of labeling segments in G_s is recast as an optimization problem: find the set of sulcal candidates in G_c that best match G_m. The objective function and the optimization process are described in the following.

2.5.1. Objective function

Because a slight over-segmentation resulted from the surface segmentation and splitting procedures, we need to collect segments that make up a specific sulcus. Denote as $\varphi_1, \ldots, \varphi_{n_\varphi}$ the n_φ sulci that we want to recognize, represented by the model graph G_m. $\psi_1, \ldots, \psi_{n_\varphi}$ are the n_φ sets of sulcal candidate segments of sulci $\varphi_1, \ldots, \varphi_{n_\varphi}$, which form graph G_c. One segment S can only belong to a single sulcus: $\psi_i \bigcap \psi_j = \phi, \forall\ (i,j = (1,\ldots,n_\varphi), i \neq j)$. The objective function is defined as

$$O(\psi_1, \ldots, \psi_{n_\varphi}) = O_F(\psi_1, \ldots, \psi_{n_\varphi}) O_N(\psi_1, \ldots, \psi_{n_\varphi}), \tag{8}$$

where $O_F(\cdot)$ and $O_N(\cdot)$ are unary feature- and neighborhood-based similarity values that are computed from the node features and edge connections of G_c and G_m. We assume the components of our feature vector are independently Gaussian distributed, so $O_F(\cdot)$ can be calculated as

$$O_F(\psi_1, \ldots, \psi_{n_\varphi}) = \prod_{i=1}^{n_\varphi} \left[W_{\psi_i} \prod_{j=1}^{n_f} \frac{1}{\sqrt{2\pi}\sigma_{ij}} \exp\left(-\frac{(f_{ij} - \mu_{ij})^2}{2\sigma_{ij}^2} \right) \right]. \tag{9}$$

Here, f_{ij} corresponds to the j th component of feature vector $\vec{f}_i$ of candidate ψ_i, and μ_{ij}, σ_{ij} are the mean value and standard deviation of the j th component of feature $\vec{f}_i$ of the sulcus φ_i in the model graph G_m. W_{ψ_i} represents an association measure, obtained by maximizing the weights w_S in the set of segments that make up ψ_i:

$$W_{\psi_i} = \arg\max_{S_{CE} \in \psi_i} \prod_{S \in \psi_i; S \neq S_{CE}} w_S(S_{CE}). \tag{10}$$

Here, S_{CE} is a suitably chosen center segment, and $w_S(S_{CE})$ corresponds to the largest weight w (see Eq. (4)) that connects segment S with a neighbor one level closer to the center segment node S_{CE} in the segment graph G_s (see Fig. 8). Two neighboring segments separated by high ridges and large distances receive a small association weight, so this measure prevents merging segments that do not belong to the same sulcus. Although this also penalizes a (valid) connection of interrupted sulci, the overall recognition accuracy is improved (see experimental section).

The neighborhood-based similarity $O_N(\cdot)$ compares the edge information of the candidate graph G_c with the model graph G_m:

$$O_N(\psi_1, \ldots, \psi_{n_\varphi}) = \exp\left(-\beta \sum_{i=1}^{n_\varphi} \sum_{j=1, j\neq i}^{n_\varphi} \left| e_{ij}(G_c) - e_{ij}(G_m) \right| \right), \tag{11}$$

where e_{ij} are the weights between the i th and j th nodes in graph G_c and G_m (see Eq. (7)), and β is a scaling factor. If two nodes are not neighbors, then $e_{ij} = 0$. A higher similarity in the weights between graph G_c and G_m results in a higher value of $O_N(\cdot)$.

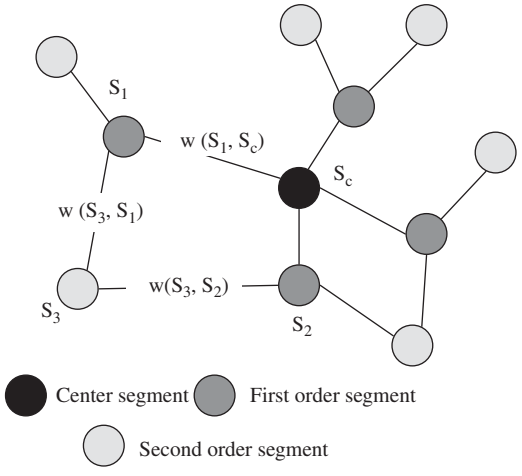

Fig. 8. An illustration of the computation of the coefficient W_ψ. For the first-order neighbor S_1 of the center segment S_c, $w_{S_1} = w(S_1, S_c)$, because there is only one link between S_1 and the center segment S_c. For the second-order node S_3, there are two links connecting it to the first-order neighbors S_1 and S_2. We select the larger one of weights $w(S_3, S_1)$ and $w(S_3, S_2)$ as w_{S_3}.

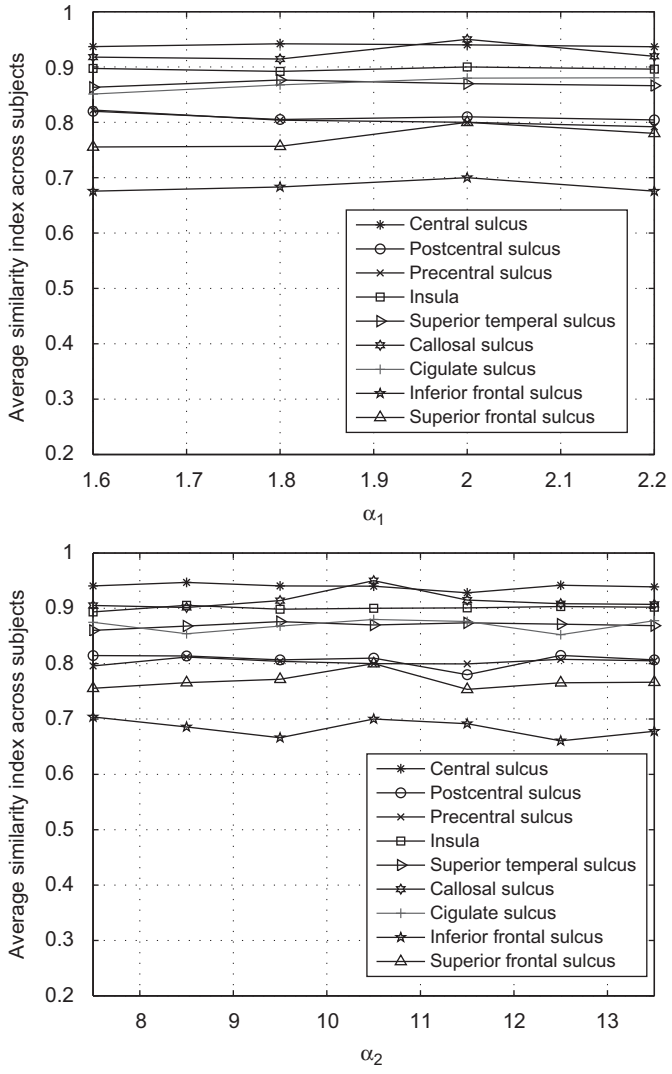

Fig. 9. Influence of the setting of α_1 (top) and α_2 (below) in Eq. (4) on the recognition rate.

Substituting Eqs. (9)–(11) into (8), log-transforming and dropping constants, we obtain our objective function:

$$O_{log} = \sum_{i=1}^{n_\varphi} \left\{ \sum_{j=1}^{n_f} \left[\frac{(f_{ij} - \mu_{ij})^2}{2\sigma_{ij}^2} \right] + \sum_{S \in \psi_i} w_S \right\} - \beta \sum_{i=1}^{n_\varphi} \sum_{j=1, j \neq i}^{n_\varphi} |e_{ij}(G_c) - e_{ij}(G_m)|. \quad (12)$$

2.5.2. Optimization

Our sulcus identification strategy aims to select a group of $\psi_1, \ldots, \psi_{n_\varphi}$ to form a candidate graph G_c that maximizes the similarity with the model graph G_m via the objective function equation (12). From the segmentation and splitting procedures, we typically obtain 100 sulcal patches [40]. Suppose we try to recognize nine sulci, and one label represents the background, then the number of possible solutions is 10^{100}. Prior knowledge about the approximate location drastically reduces the search space of the optimization problem. We exclude segments that do not belong to any of the sulci we want to identify, i.e., if the prior segment probability $P(S \in \varphi_i) = 0$ for all $i = 1, \ldots, n_\varphi$, we exclude S. Currently, we use a genetic algorithm (GA) [8] to solve this complex combinatorial optimization problem. GA try to mimic the biological evolution process. A solution of the optimization problem that fits the objective function better has a higher chance to survive and produce offsprings. Other optimization strategies (e.g., probability relaxation [4]) are viable but untested alternatives.

Suppose we have n_s candidate segments from which we want to assemble n_φ sulci. A solution of the sulcus identification problem can be represented as a string of n_s *genes* $(g_1, \ldots, g_{n_s})$. Each gene contains the current labeling of a candidate segment as an integer label between 0 and n_φ, and 0 denotes a null assignment. The optimization procedure is outlined as follows:

- Initialization: A *population* of N_c members is formed that represent initial solutions. In each member, genes g_i are assigned an integer value $k \in [0, n_\varphi]$ with a probability equal to $1 - \sum_{j=1}^{n_\varphi} P(S_i \in \varphi_j)$ for $k = 0$ and $P(S_i \in \varphi_k)$ for k in $[1, n_\varphi]$. The value of the objective function (Eq. (12)) is computed for each member and stored as its fitness.
- Selection: A subset of the current population is selected to produce offspring solutions. We choose $N_c R_p$ members from the current population to form a temporary population, where R_p is the replacement ratio. A member is selected with a probability equal to its fitness divided by the sum of the fitness of all members in the population.
- Crossover: The crossover operator exchanges a part of the solution between member pairs. Randomly select $N_c R_p P_c/2$ member pairs from the temporary population, where P_c is the crossover probability. Exchange two substrings of the same length in a pair at a randomly selected location in $[0, n_s]$.
- Mutation: The mutation operator modifies a single solution. Randomly select $N_c R_p P_m$ members from the temporary population,where P_m is the mutation probability. Select a gene i randomly from $[1, n_s]$ and assign a new label k with a probability equal to $1 - \sum_{j=1}^{n_\varphi} P(S_h \in \varphi_j)$ for $k = 0$ and $P(S_h \in \varphi_k)$ for k in $[1, n_\varphi]$.
- Update: Add the $N_c R_p$ members in the temporary population to the current population. Compute the fitness of the newly created members. Remove the $N_c R_p$ worst members to form the next generation.
- Termination: If the fitness values of the best and worst members of the current generation are equal, terminate. Else go to step "selection".

We use a population size of 1000 members, a replacement ratio $R_p = 0.4$, a crossover probability $P_c = 0.9$, and a mutation rate $P_m = 0.3$.

3. Experiments

From a large database of healthy subject (see [14] for a complete demographic description), we randomly selected 40 cases (27.6 ± 11.09 years, 15 males, 25 females). Subjects were scanned on a Bruker 3T Medspec 100 system, equipped with bird cage quadrature coil. T_1-weighted images were acquired using a 3D modified driven equilibrium Fourier transform (MDEFT) protocol: field-of-view $220\,\text{mm} \times 220\,\text{mm} \times 192\,\text{mm}$, matrix $256 \times 256 \times 128$, $\text{TR} = 1.3\,\text{s}$, $\text{TE} = 10\,\text{ms}$, voxel size $0.9\,\text{mm} \times 0.9\,\text{mm} \times 1.5\,\text{mm}$.

Cortical surfaces corresponding to the WM/GM interfaces were generated, and cut into right and left hemispheres using the surface generation method described above. Our sulcus recognition method was performed on 40 right hemispheres. We focus on the recognition of the insula (INS), the central (CS), postcentral (PTS), precentral (PCS), superior temporal (STS), callosal (CLS),

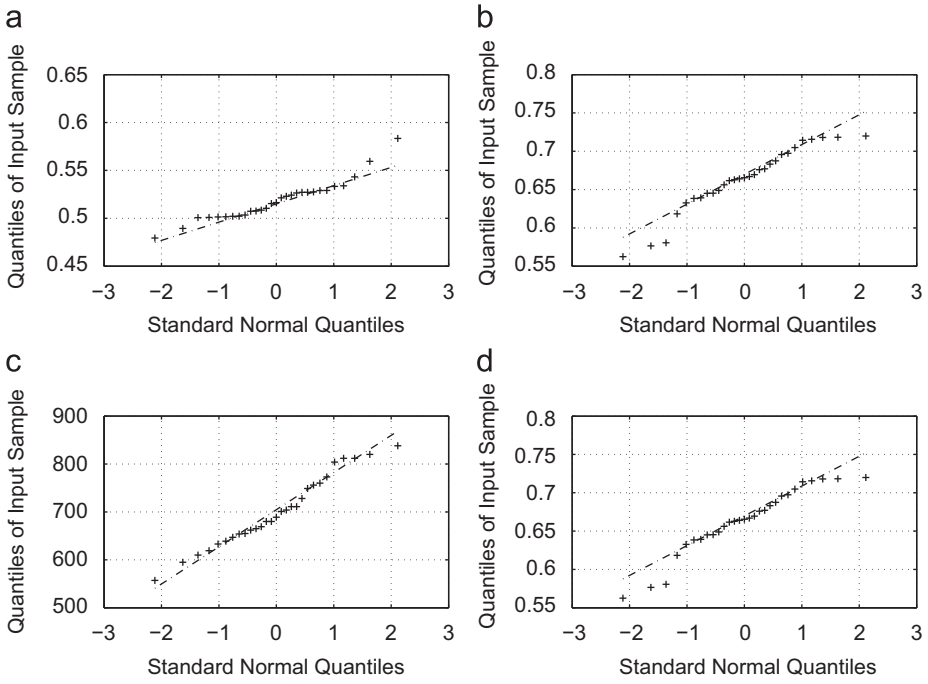

Fig. 10. QQ-plots of example feature vector components: (a) c_x; (b) d_z; (c) I_1 and (d) I_4.

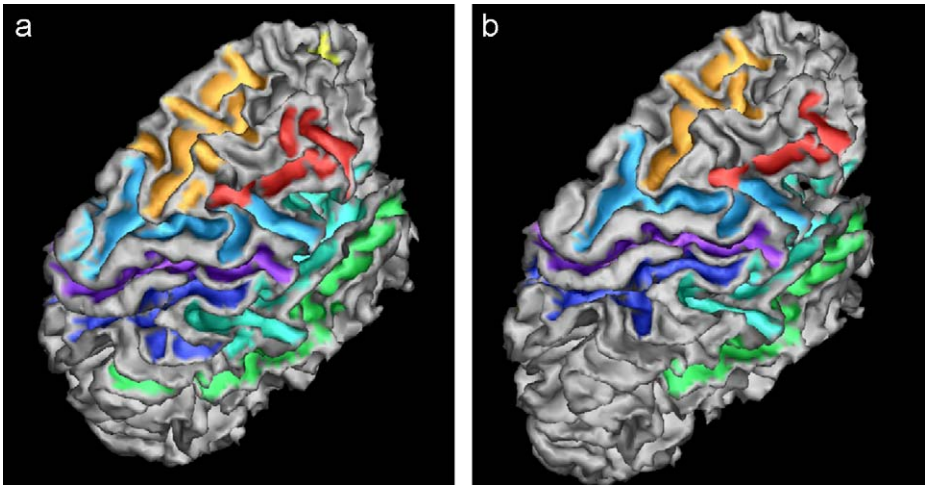

Fig. 11. Influence of the association measure W_{ψ_i} in the objective function (without W_{ψ_i} (a) and with W_{ψ_i} (b)). Some secondary sulci near the SFS and IFS are included in (a) but correctly omitted if the association measure is used (b).

cingulate (CIS), superior frontal (SFS) and inferior frontal sulcus (IFS). These nine sulci are well-defined and comprise the major sulci on the lateral and medial cortical surfaces.

An expert labeled these sulci by selecting, merging, and cutting automatically generated sulcal segments on the WM/GM interface mesh in all 40 cases. A leave-one-out strategy was pursued for validation: 39 datasets were used to build the spatial map and the model graph G_m and the remaining dataset was used for testing. To rate the correctness of the automatical labeling procedure, the true positive rate (*TPR*), false positive rate (*FPR*), and the similarity index (*SI*) of each sulcus are computed:

$$\mathrm{TPR} = \frac{TP}{TP + FN}, \tag{13}$$

$$\mathrm{FPR} = \frac{FP}{FP + TN}, \tag{14}$$

$$\mathrm{SI} = \frac{2TP}{2TP + FP + FN}, \tag{15}$$

where *TP* corresponds to the number of vertices of a specific sulcus that were correctly labeled by our algorithm, *FN* is the number of vertices that belong to this sulcus but were unlabeled, *FP* is the number of vertices falsely labeled as this sulcus, and *TN* is the number of vertices that do not belong to this sulcus and are unlabeled. Average rates across sulci and subjects are reported.

Our first experiment evaluates the relative influence of the weights for ridge height (α_1) and inter-segment distance (α_2) in the segment collection process (see Eq. (4)). We varied (1) α_1 from 1.6 to 2.2 in steps of 0.2 with a fixed setting $\alpha_2 = 10.5$ and (2) α_2 from 7.5 to 13.5 in steps of 1.0 with a fixed setting of $\alpha_1 = 2.0$. The average *SI* (across subjects) for each sulcus is shown in Fig. 9. Identification results are stable against the setting of these parameters. In the following experiments, we use $\alpha_1 = 2.0$ and

$\alpha_2 = 10.5$. From a similar experiment, we selected $\beta = 10$, with a range of [5, 15].

We tested the distribution of several features in our training samples. In Fig. 10, quantiles of the sample data vs. the standard normal quantiles are listed for the central sulcus. Because quantile–quantile plots are almost linear, we conclude that our normality assumption is reasonable.

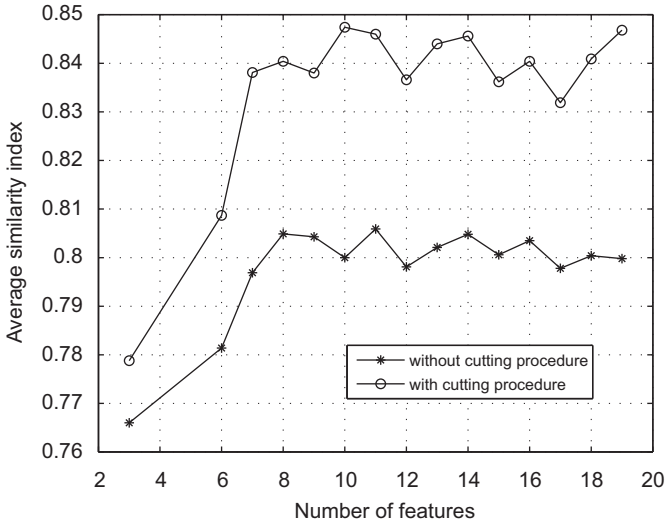

Fig. 12. The average similarity index vs. the number of features with and without the application of the cutting procedure.

Table 1
Average *TPR*, *FPR* and *SI* with and without cutting procedure for the central sulcus (CS), postcentral sulcus (PTS), precentral sulcus (PCS), insula (INS), superior temporal sulcus (STS), callosal sulcus (CLS), cingulate sulcus (CIS), superior frontal sulcus (SFS), and inferior frontal sulcus (IFS).

Sulcus	*TPR* (%)	*FPR* (%)	*SI* with cutting (%)	*SI* w/o cutting	*p*-Value
CS	94.5	0.2	0.94±0.07	0.95±0.06	n.s.
PTS	87.3	0.7	0.81±0.16	0.82±0.15	n.s.
PCS	79.9	0.5	0.80±0.13	0.71±0.15	0.0014
INS	90.0	0.6	0.90±0.04	0.90±0.05	n.s.
STS	88.6	0.5	0.87±0.09	0.87±0.10	n.s.
CLS	93.7	0.1	0.95±0.11	0.93±0.12	n.s.
CIS	91.5	0.7	0.88±0.09	0.87±0.10	n.s.
IFS	74.5	0.7	0.70±0.18	0.61±0.28	0.0275
SFS	85.0	0.4	0.80±0.17	0.55±0.32	4.4626e−5

Significance values in the rightmost column demonstrate the improvement of the cutting procedure for the precentral, superior frontal, and inferior frontal sulci.

Next, we tested the influence of the segment association measure W_{ψ_i} (see Eq. (10)) on sulcus recognition. Leave-one-out experiments were performed with and without W_{ψ_i}, and resulted in slightly higher similarity indices (0.8474 vs. 0.84) if W_{ψ_i} was included. Without this association measure, some secondary sulci tend to join with neighboring major sulci (see Fig. 11). This term is included to prevent merging neighboring sulci that do not belong to the same anatomical entity. It may, however, also penalize the intended merging of interrupted sulci. According to our experience based on this subject group, the net effect of this parameter is positive.

We evaluated the influence of specific elements of the feature vector on the recognition results. We conducted runs including the location only ($n_f = 3$), adding the principal axis ($n_f = 6$), and adding an increasing number of moment invariant features ($n_f = 7 - 19$). The average similarity index vs. the number of features n_f is shown in Fig. 12. Location, orientation, and the first four moment invariants $I_1, \ldots, I_4$ are most relevant for recognizing sulci. Including higher order invariants slightly deteriorates the performance, because they are more susceptible to (structural) noise. Including the cutting procedure yields a considerable and consistent improvement in the average *SI*.

The average *TPR*, *FPR*, and *SI* (with and without cutting) using features location, orientation, and moment invariants $I_1, \ldots, I_4$ are tabulated in Table 1 for each sulcus. Structures with a higher variability (e.g., IFS) have lower *TPR* and *SI* than rather invariant sulci (e.g., CS). A paired *t*-test between *SI*-values revealed that the cutting procedure is effective in PCS, SFS, and IFS, which is very much expected. Mean μ and standard deviation σ of sulcal features obtained from our database are listed for each sulcus in Table 2.

A quantitative comparison with other sulcus identification methods is highly desirable, but not easily accomplished. Sulci were represented by very different representations (e.g., external curves [29], bottom lines [19,12,33,38], medial surfaces [9,28], cortical surface patches [3]) that lead to different quality measures. Because Behnke et al. [3] also used sulcal segments, we compare our recognition results for those sulci that were studied with their method. They reported the *TPR* (see Eq. (13)) and the false alarm rate FAR = FP/(TP + FP). Table 3 provides a comparison for five sulci. Although our average FAR is slightly higher, our average *TPR* is considerably better. Note that our results are based on a much larger sample (40 vs. 10 subjects), which indicates a good robustness of our approach.

We implemented a sulcus identification scheme based on a probabilistic atlas as proposed by [9,37]. Again, a leave-one-out strategy was performed on the sample of 40 subjects. Measures *TPR*, *FPR*, and *SI* are compiled in comparison for our and the atlas-based approach in Table 4. Our method achieves an average *SI* 0.85 over 0.72 for the probabilistic approach. We observe a similar

Table 2
Mean μ and standard deviation σ of sulcal features obtained in the subject sample for the central sulcus (CS), postcentral sulcus (PTS), precentral sulcus (PCS), insula (INS), superior temporal sulcus (STS), callosal sulcus (CLS), cingulate sulcus (CIS), superior frontal sulcus (SFS), and inferior frontal sulcus (IFS).

	CS	STS	INS	PCS	PTS	CIS	CLS	SFS	IFS
c_x	0.52±0.02	0.72±0.03	0.60±0.02	0.50±0.04	0.52±0.04	0.15±0.01	0.09±0.02	0.33±0.04	0.59±0.04
c_y	0.03±0.02	0.09±0.02	−0.05±0.01	−0.07±0.02	0.10±0.03	−0.03±0.04	−0.03±0.04	−0.21±0.03	−0.24±0.03
c_z	−0.39±0.02	−0.04±0.03	−0.07±0.02	−0.36±0.04	−0.41±0.03	−0.31±0.03	−0.18±0.03	−0.36±0.4	−0.13±0.04
d_x	0.64±0.04	0.03±0.05	0.23±0.06	0.55±0.09	0.68±0.04	0.00±0.02	0.02±0.04	0.12±0.17	0.00±0.16
d_y	−0.40±0.07	−0.72±0.08	0.85±0.06	−0.35±0.10	−0.43±0.09	0.93±0.03	0.98±0.02	0.85±0.05	−0.67±0.13
d_z	0.65±0.05	0.68±0.09	−0.47±0.08	0.75±0.06	0.59±0.08	−0.35±0.08	−0.12±0.14	−0.45±0.15	0.70±0.16
I_1	693±76	888±137	1640±180	711±115	581±96	1040±159	271±73	465±104	451±124
I_2	5.76±0.80	6.74±1.47	4.39±0.63	5.29±0.76	5.31±1.22	13.68±2.07	18.93±2.81	4.80±1.20	3.86±0.60
I_3	2.83±0.80	4.86±1.60	4.19±1.09	3.58±0.76	3.41±1.29	17.90±5.54	31.10±12.13	3.29±1.01	3.15±0.90
I_4	0.33±0.16	0.90±0.41	1.07±0.41	0.63±0.20	0.56±0.33	1.45±0.71	4.02±4.51	0.54±0.20	0.58±0.27

Table 3
Recognition results for our method and Behnke's [3]: central sulcus (CS), insula (INS), superior temporal sulcus(STS), cingulate sulcus (CIS), superior frontal sulcus (SFS) on the right hemisphere.

	TPR		*FAR*	
	Our method (%)	Behnke's method (%)	Our method (%)	Behnke's method (%)
CS	94.5	100	5.9	5.8
INS	90.2	92	7.9	6
STS	89.3	83.6	12.6	12.9
SFS	85.1	72.8	21	29.7
CIS	91.7	74.7	14.2	2.1
Avg. over sulci	90.2	84.6	12.3	11.3

Table 4
Recognition results for our method and a scheme based on a probabilistic atlas: central sulcus (CS), postcentral sulcus (PTS), precentral sulcus (PCS), insula (INS), superior temporal sulcus (STS), callosal sulcus (CLS), cingulate sulcus (CIS), superior frontal sulcus (SFS), and inferior frontal sulcus (IFS).

	Our method			Probability atlas-based strategy		
	TPR (%)	FPR (%)	*SI* (%)	*TPR* (%)	*FPR* (%)	*SI*
CS	94.5	0.2	0.94	94.1	0.2	0.94
PTS	87.3	0.7	0.81	71	0.4	0.72
PCS	79.9	0.5	0.80	47.9	0.6	0.52
INS	90.0	0.6	0.90	88.9	0.6	0.89
STS	88.6	0.5	0.87	85.0	0.6	0.85
CLS	93.7	0.1	0.95	54.0	0.02	0.55
CIS	91.5	0.7	0.88	85.1	0.6	0.85
IFS	74.5	0.7	0.70	56.7	0.4	0.56
SFS	85.0	0.4	0.80	59.4	0.4	0.61
Avg. over sulci	87.2	0.5	0.85	71.3	0.4	0.72

performance for both methods in relatively invariant sulci (e.g., central sulcus, insula). This is straightforward to understand, because probabilistic information is much sharper in these sulci.

Finally, let us discuss some problems of our procedure based on an example subject (Fig. 13) with smallest similarity index measure (0.7428). Compared with the manually labeled sulci, some secondary sulci are attached to the primary sulci: blue patches (in the white ellipses) are attached to the PCS. A portion of the STS (in the white ellipse) is missing. Some small segments are wrongly identified (the red segments in the white ellipses). The main reason for these errors is the considerable variability of the sulcus pattern across subjects. Segmentation errors during surface generation are another possible source for identification errors. Finally, the optimization process will only yield a result that is close to optimal in a limited amount of time. However, even for this worst case, all major sulci are correctly labeled.

To further provide a visual impression of the identification results, we include identification results for two cases in Fig. 14, which are selected randomly from the 40 subjects.

Algorithms were implemented using C++ language, and tested on a Linux server with an AMD Athlon 64 processor (2.21 GHz) and 4 GB memory. All processing stages do not require user interaction, other than a visual quality check. Steps for surface generation and optimization from MRI datasets require about 50 min processing time, the segmentation into cortical patches about 20 min. The labeling procedure described here needs about an hour of computation time. There is a certain variability (about 30%) in the processing time across subjects, due to differences in the complexity of the surface and the number of surface patches.

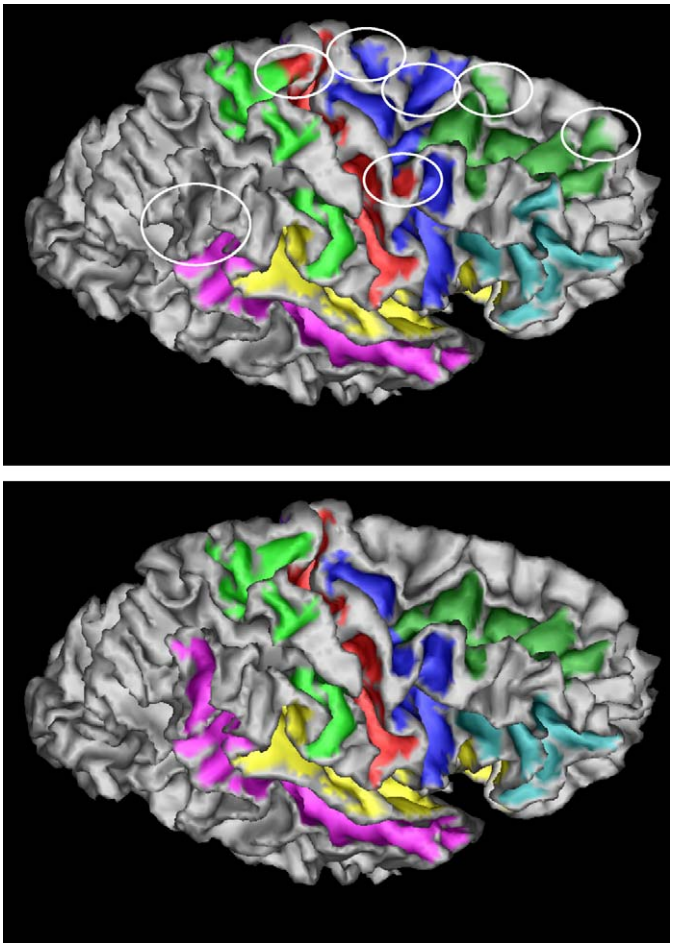

Fig. 13. Automatical (top) and manual labeling results (below) in a subject with smallest *SI* of the 40 test subjects.

4. Discussion

We introduced a novel, automatical approach for identifying major sulci that uses prior statistical information about location, orientation, shape and neighborhood structure. These features are verified as effective for characterizing sulci. Labeling is recast as a graph matching problem between a model graph of sulcal features and their neighborhood relationships and a candidate graph composed of sulcal segments obtained in a specific dataset. The combinatorial optimization problem is solved using a genetic algorithm.

Sulcus segmentation techniques based on surface features such as curvatures and geodesic depths [27,40] cannot provide a one-to-one correspondence between sulcal segments and

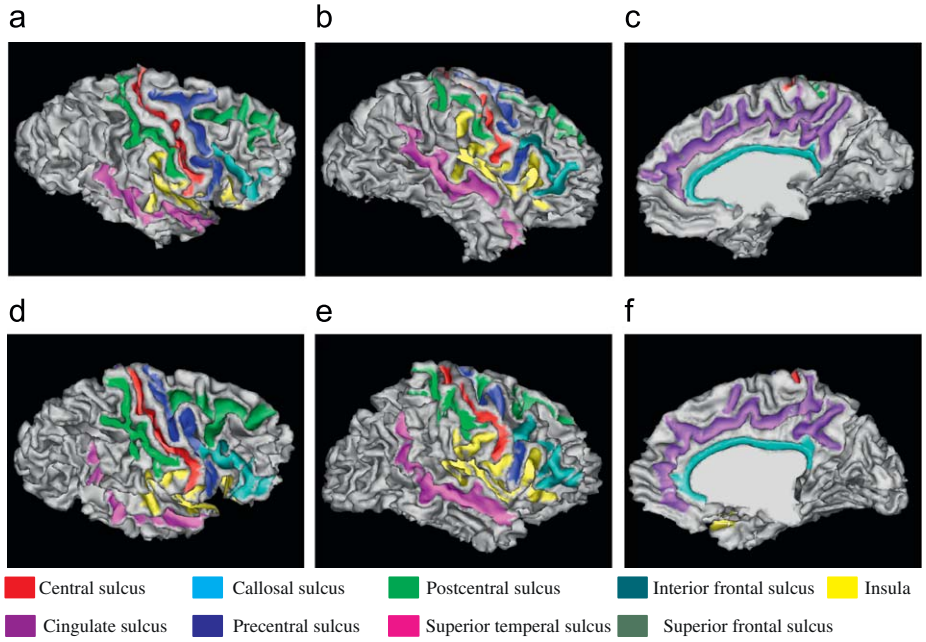

Fig. 14. Identification results for two subjects.

anatomically defined sulci. Even major sulci are interrupted with a considerable incidence while others are connected [24]. So the initial segmentation must be re-processed to merge interrupted and split connected sulci for a successful recognition. Both operations require the application of prior knowledge. Merging is usually easier, because a successful merge operation will increase the similarity between a union of candidate segments and a model sulcus, even if there is some variance in the structural features describing a sulcus. Splitting requires not only to identify a candidate segment but also to determine a suitable cut line precisely. We propose a data-driven segment-splitting scheme that uses a spatial distribution model of sulci to identify such candidate segments. The cut line is determined from individual shape features of this segment, and thus independent of the spatial uncertainty of the atlas. Given a more complete model graph G_m, a decision about segment splits may also be derived during the graph matching and optimization process.

To validate our method, we used the similarity index that represents how well the automatically recognized region matches with expert-identified sulci. To guarantee an objective validation, manual labeling and segment splitting were performed independently and without referencing automatical splitting results.

Currently, we model shape, location, and orientation features of the sulcus as independent Gaussian distributions, which we consider as a viable simplification that is justified by a good identification performance. While it is possible to model the distribution of features by a multivariate Gaussian distribution, the estimation of distribution parameters is less robust even if a much larger training sample is employed. Our current choice provides a fairly good balance between robustness and model complexity.

For optimizing the combinatorial problem of graph matching, it is straightforward to use a genetic algorithm. The segmentation procedure typically yields about 100 sulcal segments per hemisphere, so the search space for recognizing nine sulci is about 10^{100}. To reduce this dimensionality, we use prior knowledge about the spatial distribution of candidate segments, and eliminate those that are unlikely to belong to any of our target sulci. With no loss of generality, other and potentially more efficient graph matching strategies can be used here (e.g., probability relaxation [4]), and this is part of our current work.

However, a more elaborate strategy is required for more complex identification models that cover all primary and secondary sulci. Since the neighborhood relationships are sparse (e.g., an occipital sulcus is never expected to be a neighbor of a frontal sulcus), splitting a hemispheric surface first into four subregions (roughly, the frontal convexity, the medial surface, the temporal lobe, and the parieto-occipital lobe) can be achieved. For the frontal lobe and the medial surface of the brain, this idea is rather straightforward to implement by identifying a few relatively invariant key points on the surface. It remains to be seen whether a split of the temporo-parieto-occipital convexity is necessary and/or feasible. Such a segmentation provides the following advantages: at this lobular level, only 20–30 segments have to be matched with 5–10 sulci. Without loss of generality, this identification context can be used on the lobular level. Due to the drastically reduced search space, a much lower computational burden is expected for this hierarchical model.

Any attempt to capture structures of the human brain in the form of an atlas has to face the challenge posed by its complexity and variability. To overcome difficulties with techniques based on spatial normalization and image-based brain volume warping [7,32], several alternative approaches were proposed that perform a structural matching at a higher level of abstraction. Automatic sulcus identification was addressed in [35,20,28,9] using a probabilistic atlas, point distribution and shape models, neural networks and statistical models. Fischl et al. [6] use the local geometry (average complexity and curvature) and prior knowledge about the spatial distribution of sulci in their sulcus recognition procedure. We take advantage of global sulcus characteristics such as orientation and shape. Lohmann et al. [20] described a method to detect sulcal basins that correspond to substructures of a sulcus as single points. We try to recognize the whole sulcus instead, which addresses the neurobiological question. Sulci are represented by curves in [35,26], while we represent sulci using 3D surfaces on the cortex, which is more convenient for morphometry of the cortical sulci.

It is likely that no single approach is able to solve the atlas problem, but rather a combination of segmentation in the

individual data space, use of prior probabilistic (spatial) information, and symbolic knowledge about object features and their neighborhood relationships is successful. The procedure described here is an initial attempt to combine these approaches, and a resulting average similarity index of 0.85 is very encouraging.

Our aim is to develop an automatical segmentation, matching, and interpretation system for the neocortical surface. This tool for the neuroscientist will improve the understanding of the structural and functional organization of the human brain and allow morphometric analyses of brains affected by disease processes.

References

[1] S. Angenent, S. Haker, A. Tannenbaum, R. Kikinis, On the Laplace–Beltrami operator and brain surface flattening, IEEE Transactions on Medical Imaging 18 (1999) 700–711.

[2] S. Baase, Computer Algorithms: Introduction to Design and Analysis, third ed., Addison-Wesley, Reading, 2000.

[3] K.J. Behnke, M.E. Rettmann, D.L. Pham, D. Shen, S.M. Resnick, C. Davatzikos, J.L. Prince, Automatic classification of sulcal regions of the human brain cortex using pattern recognition, in: Proceedings of SPIE: Image Processing, vol. 5032, San Diego, CA, USA, 2003.

[4] W.J. Christmas, J. Kittler, M. Petrou, Structural matching in computer vision using probabilistic relaxation, IEEE Transactions on Pattern Analysis and Machine Intelligence 17 (1995) 749–764.

[5] P. Cignoni, F. Ganovelli, C. Montani, R. Scopigno, Reconstruction of topologically correct and adaptive trilinear isosurfaces, Computers & Graphics 24 (2000) 399–418.

[6] B. Fischl, A. van der Kouwe, C. Destrieux, E. Halgren, F. Ségonne, D.H. Salat, E. Busa, L.J. Seidman, J. Goldstein, D. Kennedy, V. Caviness, N. Makris, B. Rosen, A.M. Dale, Automatically parcellating the human cerebral cortex, Cerebral Cortex 14 (2004) 11–22.

[7] K.J. Friston, J. Ashburner, C.D. Frith, J.-B. Poline, J.D. Heather, R.S.J. Frackowiak, Spatial registration and normalization of images, Human Brain Mapping 3 (1995) 165–189.

[8] D.E. Goldberg, Genetic Algorithms in Search, Optimization and Machine Learning, Addison-Wesley, Reading, 1989.

[9] G.L. Goualher, D.L. Collins, C. Barillot, A.C. Evans, Automatic identification of cortical sulci using a 3D probabilistic atlas, in: Lecture Notes In Computer Science, vol. 1496, Springer, Berlin, 1998, pp. 509–518.

[10] G.L. Goualher, E. Procyk, D.L. Collins, R. Venugopal, C. Barillot, A.C. Evans, Automated extraction and variability analysis of sulcul neuroanatomy, IEEE Transactions on Medical Imaging 18 (1999) 206–217.

[11] X. Han, D.L. Pham, D. Tosun, M.E. Rettmann, C. Xu, J.L. Prince, CRUISE: cortical reconstruction using implicit surface evolution, Neuroimage 23 (2004) 997–1012.

[12] C.-Y. Kao, M. Hofer, G. Sapiro, J. Stern, K. Rehm, D.A. Rottenberg, A geometric method for automatic extraction of sulcal fundi, IEEE Transactions on Medical Imaging 26 (2007) 530–540.

[13] F. Kruggel, Techniques in analyzing the neocortial fine-structure, in: C.T. Leondes (Ed.), Medical Imaging Systems, vol. 5, , 2005, pp. 255–279.

[14] F. Kruggel, MRI-based volumetry of head compartments: normative values of healthy adults, Neuroimage 30 (2006) 1–11.

[15] F. Kruggel, Robust parametrization of brain surface meshes, Medical Image Analysis 12 (2008) 291–299.

[16] F. Kruggel, D.Y. von Cramon, Alignment of magnetic-resonance brain datasets with the stereotactical coordinate system, Medical Image Analysis 3 (1999) 175–185.

[17] C.-H. Lo, H.-S. Don, 3-D moment forms: their construction and application to object identification and positioning, IEEE Transactions on Pattern Analysis and Machine Intelligence 11 (1989) 1053–1064.

[18] G. Lohmann, Extracting line representations of sulcal and gyral patterns in MR images of the human brain, IEEE Transactions on Medical Imaging 17 (1998) 1040–1048.

[19] G. Lohmann, F. Kruggel, D. Y. von Cramon, Automatic detection of sulcal bottom lines in MR images of the human brain, in: Processing in Medical Imaging, Lecture Notes in Computer Science, vol. 1230, Springer, Berlin, 1997, pp. 369–374.

[20] G. Lohmann, D.Y. von Cramon, Automatic labelling of the human cortical surface using sulcal basins, Medical Image Analysis 4 (2000) 179–188.

[21] J.-F. Mangin, V. Frouin, I. Bloch, J. Régis, J. López-krahe, From 3D magnetic resonance images to structural representation of the cortex topography using topology preserving deformations, Journal of Mathematical Imaging and Vision 5 (1995) 297–318.

[22] J.-F. Mangin, F. Poupon, E. Duchesnay, D. Rivière, A. Cachia, D.L. Collins, A.C. Evans, J. Régis, Brain morphometry using 3D moment invariants, Medical Image Analysis 8 (2004) 187–196.

[23] F. Meyer, S. Beucher, Morphological segmentation, Journal of Visual Communication and Image Representation 1 (1990) 21–46.

[24] M. Ono, S. Kubik, C.D. Abernathey, Atlas of the Cerebral Sulci, Georg Thieme Verlag, New York, 1990.

[25] D.L. Pham, J.L. Prince, Adaptive fuzzy segmentation of magnetic resonance images, IEEE Transactions on Medical Imaging 18 (1999) 737–752.

[26] J. Regis, Anatomie sulcale profonde et cartographie fonctionnelle du cortex cérébral, Ph.D. Thesis, de doctorat de la faculté de médecine de marseille, 1994.

[27] M.E. Rettmann, X. Han, C. Xu, J.L. Prince, Automated sulcal segmentation using watersheds on the cortical surface, Neuroimage 15 (2002) 329–344.

[28] D. Rivière, J.-F. Mangin, D. Papadopoulos-Orfanos, J.-M. Martinez, V. Frouin, J. Régis, Automatic recognition of cortical sulci of the human brain using a congregation of neural networks, Medical Image Analysis 6 (2002) 77–92.

[29] N. Royackkers, H. Fawal, M. Desvignes, M. Revenu, J.-M. Travère, Feature extraction for cortical sulci identification, in: Ninth Scandinavian Conference on Image Analysis, Uppsala, 1995.

[30] D. Shaked, A.M. Bruckstein, Pruning medial axes, Computer Vision and Image Understanding 69 (1998) 156–169.

[31] D.W. Shattuck, R.M. Leahy, Automated graph-based analysis and correction of cortical volume topology, IEEE Transactions on Medical Imaging 20 (2001) 1167–1177.

[32] D. Shen, C. Davatzikos, Hammer: hierarchical attribute matching mechanism for elastic registration, IEEE Transactions on Medical Imaging 21 (2002) 1421–1439.

[33] Y. Shi, Z. Tu, A. Reiss, R.A. Dutton, A.D. Lee, A. Galaburda, I. Dinov, P.M. Thompson, A.W. Toga, Joint sulci detection using graphical models and boosted priors, in: Information Processing in Medical Imaging, Lecture Notes in Computer Science, vol. 4584, Springer, Berlin, 2007, pp. 98–109.

[34] Z.Y. Sun, D. Rivière, F. Poupon, J. Régis, Automatic inference of sulcus patterns using 3D moment invariants, in: MICCAI, Lecture Notes in Computer Science, vol. 4791, Springer, Berlin, 2007, pp. 515–522.

[35] X. Tao, J.L. Prince, C. Davatzikos, Using a statistical shape model to extract sulcul curves on the outer cortex of the human brain, IEEE Transactions on Medical Imaging 21 (2002) 513–524.

[36] P. Thévenaz, T. Blu, M. Unser, Image interpolation and resampling, in: Handbook of Medical Image Processing, 2000.

[37] D. Tosun, M.E. Rettmann, J.L. Prince, Mapping techniques for aligning sulci across multiple brains, Medical Image Analysis 8 (2004) 295–309.

[38] Z. Tu, S. Zheng, A.L. Yuille, A.L. Reiss, R.A. Dutton, A.D. Lee, A.M. Galaburda, I. Dinov, P.M. Thompson, A.W. Toga, Automated extraction of the cortical sulci based on a supervised learning approach, IEEE Transactions on Medical Imaging 26 (2007) 541–552.

[39] F. Vivodtzev, L. Linsen, B. Hamann, K.I. Joy, B.A. Olshausen, Brain mapping using topology graphs obtained by surface segmentation, in: Scientific Visualization: The Visual Extraction of Knowledge from Data, Springer, Berlin, Heidelberg, 2006, pp. 35–48.

[40] F. Yang, F. Kruggel, Automatic segmentation of human brain sulci, Medical Image Analysis 12 (2008) 442–451.

[41] Y. Zhou, P.M. Thompson, A.W. Toga, Extracting and representing the cortical sulci, IEEE Computer Graphics and Applications 19 (1999) 49–55.

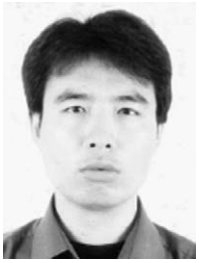

Faguo Yang received his B.Sc. degree in mechatronic engineering and M.Sc. degree in mechanical engineering and automation from Beijing Institute of Technology, China, in 1997 and 2000, respectively. He obtained his Ph.D. degree from National Lab of Pattern Recognition, Institute of Automation, Chinese Academy of Sciences, in 2003. Now he is a post-doc researcher in Signal and Image Processing Lab, Department of Biomedical Engineering, University of California, Irvine. His research interests include medical image analysis, computer vision, pattern recognition.

Frithjof Kruggel studied Chemistry and Medicine in Bochum and Munich (Germany), and was trained in Clinical Neurology and Neuropsychology. In 1995, he assisted in building up the newly founded Max-Planck-Institute of Cognitive Neuroscience, where he headed the Workgroup on Signal and Image Analysis from 1995 to 2004. He joined the Department of Biomedical Engineering at UC Irvine in 2005. Dr. Kruggel focuses on computational neuroanatomy and human brain mapping. He develops methods to describe individual brain structures by meaningful quantitative characteristics such as size, shape, and texture.